PREDICTION OF A SUBCOOLED BOILING FLOW WITH MECHANISTIC WALL BOILING AND BUBBLE SIZE MODELS

B.J. Yun[*], A. Splawski[†], S. Lo[†], and C.–H. Song [*]

[*] *Thermal Hydraulics Safety Research Division, Korea Atomic Energy Research Institute, Daejeon, 305-353, Korea*

[†] *CD-adapco, Trident House, Basil Hill Road, Didcot OX11 7HJ, UK*

Abstract

In order to enhance the prediction capability of subcooled boiling flows, an advanced wall boiling model and mechanistic bubbles size model were examined using a CFD (Computational Fluid Dynamics) code. The advanced wall boiling model consists of a mechanistic bubble departure size model (Klausner et al., 1993), Hibiki et al.'s (2009) active nucleate site density model and Cole's (1960) bubble departure frequency model. To ensure a wide range applicability of the advanced wall boiling model, each sub-model was evaluated separately over a wide range of flow conditions in pressure, temperature and flow rate. Finally, the advanced wall boiling model was implemented into the commercial CFD code STAR-CD via user FORTRAN files.

For an accurate prediction of bubble size which governs interfacial transfer terms between the two phases, the S_γ model (Lo et al., 2009) was also applied.

The benchmark calculation against the DEBORA subcooled boiling data confirms that the new mechanistic wall boiling and bubble size models follow well the tendency on the change of flow conditions and are applicable to the wide range of flow conditions that are expected in the nominal and postulated accidental conditions of a nuclear power plant.

1. INTRODUCTION

Accurate simulation of subcooled boiling flow is essential for the operation and safety of nuclear power plants (NPP). Recently, there are two new examples for such simulations in the Korean nuclear industry. One is a subcooled boiling phenomena on the top of nuclear fuel rods, which governs boron deposition on the surface of nuclear fuel rods during the normal operation of a PWR (Pressurized Water Reactor). The other is a downcomer boiling phenomena which results in a reduction of the reflood flow rate for the core cooling during a postulated large break loss of coolant accident (LBLOCA) of ARP1400. (Yun, 2006, Song, 2007).

However, it has been revealed that most of the 1D safety analysis codes for NPP have an inherent weakness in the prediction of subcooled boiling phenomena in which multi-dimensional flow behaviour is expected. Moreover, the need for a multi-dimensional analysis tool for the thermal-hydraulics in nuclear reactor components is further increased with the adoption of advanced safety design features such as a passive decay heat removal system in which two-phase natural convection occurs.

In recent years, the use of computational fluid dynamics (CFD) codes has been extended to the analysis of multi-dimensional two-phase flow to overcome the weakness of 1D analysis code. Among the applications of CFD code for the NPP analysis, the first target was selected as a mechanistic prediction of DNB (Departure from Nucleate Boiling) in PWR (Bestion et al, 2009). In DNB-type CHF (Critical Heat Flux), the expected flow regime is bubbly or churn turbulent flow in the high mass flux and high heat flux condition and thus subcooled boiling is also one of the key phenomena for the precise prediction of DNB.

Recently, many investigators such as Koncar et al. (2002, 2007), Yeoh et al. (2005) and Bae et al. (2010) tried to improve subcooled boiling models for CFD codes.

In this paper, an advanced wall boiling model and a mechanistic bubbles size model were examined in a CFD code with the objective of enhancing the prediction capability of subcooled boiling flows. The models were applied in the STAR-CD 4.12 software. Benchmark calculation against experimental data shows that the two models are promising for the better prediction of subcooled boiling flows.

2. ADVANCED SUBCOOLED BOILING MODEL

Most of the CFD codes adopted Eulerian multiphase flow approach based on the two-fluid model for the prediction of two phase flows. In these codes, instantaneous time averaged equations for the conservation of mass, momentum and energy are solved for each phase. However, constitutive models are required in solving of these equations such that the prediction results depend directly on the performance of these constitutive models. In the present work, new constitutive models were provided to improve a prediction capability of subcooled boiling flows.

2.1 Wall Boiling Model

At a heated wall, boiling occurs when the wall temperature exceeds the saturation temperature of liquid. In this flow condition, the bubble generation rate is determined by the wall heat partitioning model as follows,

$$q_w = q_l + q_Q + q_e \tag{1}$$

where, q_w is total heat flux from wall, q_l is the single phase convection heat flux that takes place outside the influence area of the nucleation bubbles, q_Q is quenching heat flux within the bubble influence area and q_e is evaporation heat flux at the heated wall. The bubble influence area A_e is defined by,

$$A_e = F_A \frac{\pi d_d^2}{4} N'' \tag{2}$$

where, F_A ,d_d, N'' are model constant, bubble departure size and active nucleation site density, respectively.

As shown in equation (1), the evaporation heat flux is one of the key parameters to be modelled for an accurate prediction of subcooled boiling flows. The modelling of evaporation heat flux in conventional CFD codes is expressed as follows,

$$q_e = \frac{\pi d_d^3}{6} \rho_g h_{fg} f N'' \tag{3}$$

where, ρ_g is steam density, h_{fg} is latent heat and f is bubble departure frequency.

In most commercial CFD codes, Tolubinsky (1970) bubble departure size model, Kurul & Podowski (1990) active nucleation site density model and Cole's (1960) bubble departure frequency model were adopted as a basic wall boiling model. These models have very simple forms and they do not reflect properly their dependency on the flow, pressure and fluid properties. In this paper, an advanced wall boiling model is proposed to improve the subcooled boiling model in CFD codes.

Bubble departure size model

Klausner et al. (1993) proposed a mechanistic force balance model for the prediction of both bubble departure and lift-off sizes in the nucleate boiling condition of refrigerant R113. They applied the model successfully in the various flow conditions in both horizontal and vertical channels under pool and flow boiling. Later, many investigators also tried to improve the model to achieve a general applicability for flow direction and fluids. Zeng et al. (1993a,b) applied the model for both horizontal and vertical channels under pool and flow boiling whereas Situ (2005) and Yeoh et al. (2005) extended its application to steam-water boiling flow condition.

In the present work, Klausner's force balance model was adopted to replace the Tolubinsky bubble departure model (1970). The force balance model is applied in the flow and lateral directions as follows (See Fig.1),

$$\sum F_x = F_{sx} + F_{dux} + F_{sL} + F_h + F_{cp} \tag{4}$$

$$\sum F_y = F_{sy} + F_{duy} + F_{qs} + F_b \tag{5}$$

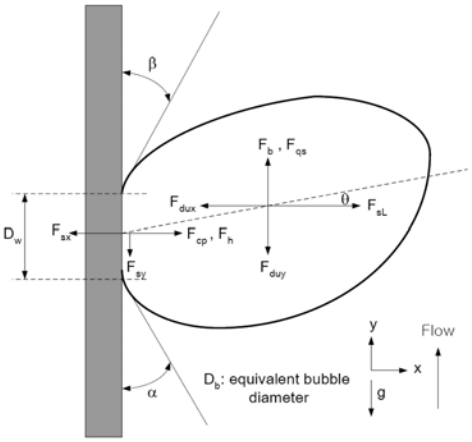

Fig.1 : Forces acting on the growing bubble from boiling site

where, F_s is the surface tension force, F_{du} the unsteady drag force due to asymmetrical growth of a stationary bubble, F_{sL} the shear lift force, F_h the force due to hydrodynamics pressure, F_{cp} the contact pressure force accounting for the bubble being in contact with a solid rather than being surrounded by liquid, F_{qs} the quasi-steady drag force in the flow direction, F_b the buoyancy force, α the advancing contact angle and β the receding contact angle.

Bubble departure occurs when the detaching forces exceed the attaching forces in either eq. (4) or (5), thus the bubble departure is determined when eq. (4) or (5) is violated.

For the prediction of bubble departure size using eqs. (4) and (5), each force term must be modelled. Basically, we followed the original modelling for the forces proposed by Klausner et al. (1993), however, some of their modeling and coefficients were improved and adjusted, respectively. The detailed modelling of each force is summarized in the Table 1.

In the original formulation of the unsteady drag force F_{du}, the bubble condensation around the growing bubble was not considered. It is valid if the liquid temperature reaches to a saturation state, however if the liquid subcooling is maintained around the growing bubble, then bubble condensation is unavoidable. In the present work, a bubble condensation model was introduced into the modeling of F_{du} to take into account of liquid subcooling effect on the top half of a growing bubble. In addition to this, the coefficient b for the force is changed from 1.76 to 1.56 by following Zuber et al. (1961). The other improvement was for the bubble foot diameter which is required for the calculation of forces. Klausner et al. recommended a constant bubble foot diameter, $d_w (= 0.09mm)$, based on their R113 data. However, it may not be valid in high pressure steam/water flows in which a smaller bubble foot diameter is expected. Moreover, the predicted departure bubble size is strongly dependent on the value of d_w. To overcome these problems, d_w is determined iteratively by introducing a constant fraction factor against growing bubble size d_b, that is, $d_w / d_b = 1/15$.

To explore and confirm the validity and applicability of the present force balance model, it was evaluated systematically over a wide range of pressure, temperature and flow rate (Yun et al., 2010). The study confirms that the present force balance model can follow well the tendency over the range of flow conditions studied.

Active nucleation site density model

For the improvement of the active nucleation site density model, Hibiki et al.'s (2009) model was adopted in the new advanced wall boiling model. Characteristics of the Hibiki et al. model is that 1) it considers a boundary condition for a wall superheating, and 2) it is validated against a great number of experimental data. Hence it guarantees a wide range applicability for the mass flow, pressure and contact angle. Hibiki et al.'s correlation is expressed as follows,

Table 1: Summary of Modelling of Forces for Force Balance Model

Force	F_x	F_y (Gravity and Flow Direction)
F_s (Surface Tension)	$F_{sx} = -d_w\sigma\frac{\pi}{\alpha-\beta}[\cos\beta-\cos\alpha]$, $\frac{d_w}{d_b}=\frac{1}{15}$	$F_{sy} = -1.25 d_w\sigma\frac{\pi(\alpha-\beta)}{\pi^2-(\alpha-\beta)^2}[\sin\alpha+\sin\beta]$
F_{du} (Unsteady Drag ,Bubble Growth)	$F_{du} = \rho_l\pi r^2(\frac{3}{2}C_s\dot{r}^2+r\ddot{r}), C_S=1, r(t)=\frac{2b}{\sqrt{\pi}}Ja\sqrt{\eta t}\left[1-\frac{q_l''\sqrt{\pi\eta t}}{2sk(T_{wall}-T_{sat})}\right]=\frac{2b}{\sqrt{\pi}}Ja\sqrt{\eta t}-\frac{bq_l''}{sh_{fg}\rho_g}t$ $Ja=\frac{\rho_l C_{pl}\Delta T_{sat}}{\rho_g h_{fg}}$, $\eta=\frac{k_l}{\rho_l C_{pl}}$, $b:1.56$, $q_l=h_l(T_{sat}-T_l), S=2, h_l=\frac{k}{d_b}(2+0.6\mathrm{Re}_d^{0.5}\mathrm{Pr}_c^{0.3})$	
	$F_{dux} = -F_{du}\cos\theta_l$	$F_{duy} = -F_{du}\sin\theta_l$
F_b (Buoyancy)	-	$F_b = \frac{4}{3}\pi r^3(\rho_l-\rho_g)g$
F_{qs} (Quasie-steady Drag)	-	$F_{qs} = 6\pi\mu_l U_l r\left[\frac{2}{3}+\{(\frac{12}{\mathrm{Re}})^n+0.796^n\}^{-1/n}\right]$, $n=0.65$ $\mathrm{Re}=\frac{\rho_l U_l d_b}{\mu_l}$
F_{sL} (Shear Lift)	$F_{sL} = (\frac{1}{2}\rho_l U_l^2\pi r^2)[3.877G_s^{1/2}(\mathrm{Re}^{-2}+0.118G_s^2)^{1/4}]$ $G_s=\left\|\frac{dU}{dy}\right\|\frac{r}{U_l}$, $\mathrm{Re}=\frac{\rho_l U_l d_b}{\mu_l}$	-
F_h (Hydrodynamic Pressure)	$F_h = \frac{9}{8}\rho_l U_l^2\frac{\pi d_w^2}{4}$	-
F_{cp} (Contact Pressure)	$F_{cp}=\frac{\pi d_w^2}{4}\frac{2\sigma}{r_r}$, $r_r(\sim 5r)$	

$$N_n = \overline{N}_n\left\{1-\exp(-\frac{\theta^2}{8\mu^2})\right\}\left[\exp\left\{f(\rho^+)\frac{\lambda'}{R_c}\right\}-1\right] \tag{6}$$

where, θ is the contact angle, $\mu = 0.722$, $\overline{N}_n = 4.72\times10^5$ sites/m^2, $\lambda' = 2.50\times10^{-6}$ m. R_c is a critical cavity radius given as,

$$R_c = \frac{2\sigma\{1+(\rho_g/\rho_f)\}/P_f}{\exp\{h_{fg}(T_g-T_{sat})/RT_gT_{sat}\}-1} \tag{7}$$

where, σ is surface tension, ρ_f is steam density, P_f is the liquid pressure R is the gas constant based on the molecular weight of fluid.

The $f(\rho^+)$ in eq. (6) is a function to consider the pressure effect on the active nucleation site density and given as,

$$f(\rho^+) = -0.01064 + 0.4824\rho^+ - 0.22712\rho^{+2} + 0.05468\rho^{+3} \tag{8}$$

where, $\rho^+ = \log(\rho^*)$, $\rho^* = \Delta\rho/\rho_g$

Hibiki et al.'s model is applicable in the range of 0.0~886 kg/m^{2}sec for mass flux, 0.101~ 19.8 MPa for pressure, 5~90^o for contact angle and 1x10^4~1.1x10^{10} sites/m^2 for active nucleation site density. For the calculation of R_c in eq. (6), superheated liquid temperature T_g near the heated wall is required. However, this temperature is not available in conventional CFD calculation, hence T_g is assumed to be the surface temperature at the heated wall, T_w in the present work.

Recently, Sakashita (2009) conducted an experimental work for the active nucleation site density in the range of 3.66~ 5 MPa for pressure and 0.05~0.35 MW/m^2 for heat flux and confirmed that Hibiki et al.'s model can predict their experimental data with 54% of average r.m.s. error.

Separate evaluation revealed that the active nucleation site density predicted by Hibiki et al.'s model is smaller than that of Kurul & Podowski's (1990) in the pressure range of 1~4 bars but becomes larger rapidly as the pressure increases. Finally, it becomes several orders of magnitude larger than the Kurul & Podowski's model in the operating pressure condition of a conventional NPP (Yun et al., 2010).

2.2 Velocity Wall Function for Boiling Two-phase Flow

It is known that conventional CFD codes over-predict both liquid and bubble velocity near the boiling wall. It is mainly caused by the fact that typical CFD codes adopted a single phase wall function for the liquid velocity near the heated wall even in subcooled boiling flows. Actually, the liquid velocity profile near the heated wall is far from the single phase flow because the growing and detaching bubbles disturb significantly the flow field in the sublayer. Recently, Koncar et al. (2007, 2008) applied two-phase velocity wall function by following Ramstorfer et al. (2005). Bae et al. (2010) also tried to overcome this problem by implementing Kataoka et al.'s (1997) boiling induced turbulence model into the turbulent viscosity term as well as $k-\varepsilon$ turbulence model. Both approaches showed clearly that the two-phase turbulence model should be improved to account for the boiling induced turbulence near the heated wall.

In the present work, a new velocity wall function is proposed by introducing a polynomial fitting equation for rough wall found in the text book of Duncan (1972) ,

$$u^+ = \begin{cases} \dfrac{1}{\kappa}\ln(Ey^+) & if \quad y^+ > y_{cr}^+ \\ u^+(y_{cr}^+)\dfrac{y^+}{y_{cr}^+} & if \quad y^+ \le y_{cr}^+ \end{cases} \tag{9}$$

where,

$$y^+ = \rho_x u_\tau y / \mu_x, \; x = l, g$$

$$E = \begin{cases} 9.0 & ,k^+ < 4 \\ e^{\kappa B'}/k_r^+ & ,4 \le k^+ < 70 \\ 30/k_r^+ & ,k^+ \ge 70 \end{cases}$$

$$k_r^+ = \frac{\rho_x k_r u_\tau}{\mu_x}$$

$$B' = 6.106 - 1.8692x + 28.545x^2 - 44.0855x^3 + 28.54657x^4 - 8.7074x^5 + 1.03894x^6$$

$$x = \log_{10}(k_r^+)$$

Here, $\kappa = 0.4$ and y_{cr}^+ is set to 11.3. The roughness height k_r for the boiling wall is obtained from Koncar et al. (2007) as follows,

$$k_r = \eta d \left(\frac{q_e}{q_w}\right)^{\varsigma} \tag{10}$$

The empirical coefficients η and ς are set to 1.0 and 0.5, respectively in the present study. The bubble diameter d in eq. (10) is obtained at $y^+ = 80$ by linear interpolation between the bubble departure diameter at the heated wall and the calculated bubble size at the first grid cell to remove any grid size effect.

Eq. (9) is applied to both steam and liquid phases to provide boundary condition for the force balance bubble departure size, $k-\varepsilon$ and wall heat transfer models.

3. MECHANISTIC BUBBLE SIZE MODEL

Interfacial transfer terms are functions of interfacial area concentration. In boiling flow calculations most CFD codes including STAR-CD use a linear interpolation between bubble diameters at two specified values of liquid subcooling for the bubble size according to Kurul & Podowski (1990). However, it was revealed that this method cannot predict well the bubble size and its distribution in subcooled boiling flows in which multi-dimensional flow behaviour is dominant (Koncar, 2002). To predict accurately the bubble size distribution, mechanistic modelling approach such as interfacial area concentration or bubble number density transport equation is needed. Ishii (1990) proposed the concept of interfacial area transport equation (Ishii et al. 2005). Lo (1996) proposed population

balance equations for the CFD code to take into account of non-uniform bubble size distribution in the two-phase flows. Recently, Yao et al. (2004) and Yeoh (2005) also applied an interfacial area transport equation and bubble number density transport equations, respectively, into CFD codes for the prediction of subcooled boiling flows. More recently, Lo (2007) applied generalized S_γ equations for the prediction of droplet size in the oil/water flow. Later, it was extended to the air/water flows (Lo, 2009) even though source and sink terms for the S_γ have the same functional forms as those for droplet flows. In the present work, S_γ model was applied for the prediction of bubble size in the subcooled boiling flows. However, model coefficients for breakup and coalescence are re-obtained for the subcooled boiling flows in the present work.

S_γ is defined as a generalized parameter for the size distribution of bubble/droplet as follows,

$$S_\gamma = nM_r = n\int_0^\infty d^\gamma P(d)d(d) \tag{11}$$

where, M_r is the moment of the size distribution, d the bubble/droplet size. $P(d)$ is the bubble/droplet size distribution.

Here, the zeroth-moment of the distribution is the number density of the bubble/droplet, $n = S_0$. The first-moment, S_1, is related to the mean diameter d_m ($=S_1/n$), the second-moment, S_2, is related to the interfacial area density a_i ($=\pi S_2$) and the third-moment, S_3, is related to the void fraction α ($=\pi S_3/6$). From these relations, the Sauter mean diameter can be calculated as follows,

$$d_{sm} = d_{32} = \frac{S_3}{S_2} = \frac{6\alpha}{\pi}\frac{1}{S_2} \tag{12}$$

Here, $P(d)$ is assumed to be a log-normal distribution. And, it requires S_1 and S_2 for the determination of distribution width (Kamp et al., 2001) and thus both moments S_1 and S_2 are solved in the present work.

The transport equation for the generalized S_γ is expressed as follows,

$$\frac{\partial S_\gamma}{\partial t} + \nabla\cdot(S_\gamma u_d) = s_{br} + s_{cl} + s_{mass} + s_{boil} \tag{13}$$

where, u_d is bubble/droplet velocity, s_{br}, s_{cl}, s_{mass}, s_{boil} are sources terms for breakup, coalescence, mass transfer and boiling, respectively.

Bubble/droplet breakup occurs due to rotational or elongation of fluid arisen by shear flow and also deformation of droplet/bubble caused by shear flow. The source term s_{br} for the bubble/droplet breakup is expressed as follows,

$$s_{br} = \int_0^\infty K_{br}(d)\Delta S_\gamma^{br} nP(d)d(d) \tag{14}$$

where, $K_{br}(d)$ is the breakup rate of a bubble/droplet size having d, $\Delta S_\gamma^{br}(d)$ is the change in S_γ due to a single breakup event of a bubble/droplet size d. If binary breakup of a bubble/droplet with equal size fragments is assumed, then eq. (14) becomes,

$$s_{br} = \int_0^\infty \frac{d^\gamma(2^{\frac{3-\gamma}{3}}-1)}{\tau_{br}(d)} nP(d)d(d) \tag{15}$$

where, $\tau_{br}(d)$ is breakup time.

In the modelling of the breakup rate, it is assumed that breakup occurs only if the bubble/droplet is larger than the critical diameter, d_{cr}, i.e., the so-called maximum stable bubble diameter. Breakup consists of viscous breakup and inertial breakup models which is applied according to flow condition and droplet/bubble size.

$$s_{br} = F_{br,1}s_{br,\nu} + F_{br,2}s_{br,i} \tag{16}$$

where, $F_{br,1}(=0.8), F_{br,2}(=0.8)$ are calibration coefficients determined from experimental data for viscous and inertial breakups, respectively. Viscous breakup is found in laminar flow and also in turbulent flows when the bubble/droplet is smaller than the Kolmogorov length scale L_k defined by,

$$L_k = \left(\frac{\nu_c^3}{\varepsilon}\right)^{1/4} \tag{17}$$

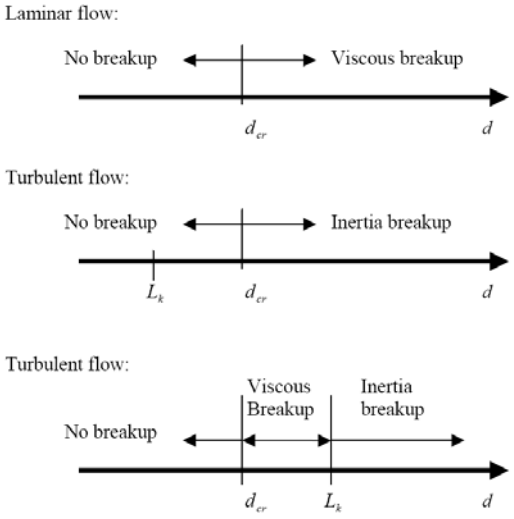

Fig. 2 : Breakup Regime for Bubble/Droplet

where ν_c is the continuous phase kinematic viscosity and ε is the continuous phase dissipation rate of turbulent kinetic energy. Larger bubbles/droplets are subjected to inertial breakup. The breakup regime is represented graphically in the Fig. 2. Detailed modelling for the viscous and inertial breakup is given by Lo et al. (2007, 2009) and summarized in the Table. 2.

Table 2: Summary of Modelling for Breakup Source Term

Viscous Regime	Inertial Regime
$d_{cr} = \dfrac{2\sigma\Omega_{cr}}{\mu_c\dot{\gamma}}$ $\Omega = \dfrac{\mu_c d}{2\sigma}\dot{\gamma}$: capillary number $\Omega_{cr} = \sqrt{\left(-\frac{c_1}{c_3}(\log\lambda)^2 - 2\frac{c_4}{c_3}\log\lambda - \frac{1}{c_3}\right) + \left(\frac{c_2}{c_3}\log\lambda + \frac{c_5}{c_3}\right)} - \frac{c_2}{c_3}\log\lambda - \frac{c_5}{c_3} - 1$ $\lambda = \mu_d/\mu_c$, c_1 to c_5 : fitting constants $\dot{\gamma}$ shear rate calculated from local velocity gradient for laminar flow $\dot{\gamma} = \sqrt{\dfrac{\varepsilon\rho_c}{\mu_c}}$: Kolomogov shear rate for turbulent flow -Breakup occurs if $\Omega \geq \Omega_{cr}$	$d_{cr} = C_{dr}(1 + C_\alpha\alpha_d)\left(\dfrac{2\sigma We_{cr}}{\rho_c}\right)^{3/5}\varepsilon^{-0.4}$ $C_{dr} = 1.0$: empirical coefficient C_α (disperse phase concentration factor) $= 4.6$ for droplet $= 0.0$ for air/water or air/steam $We = \dfrac{\rho_c u_l^2 d}{\sigma} = \dfrac{\rho_c \varepsilon^{2/3} d^{5/3}}{2\sigma}$ $We_{cr} = 0.31$ for bubble flow -Breakup occurs if $We \geq We_{cr}$
$\tau_{br} = \dfrac{\mu_c d}{\sigma} f_\tau(\lambda)$ $\log f_\tau(\lambda) = p_o + p_1\log(\lambda) + p_2(\log(\lambda))^2$ p_o, p_1, p_2 : empirical constants	$\tau_{br} = 2\pi k_{br}\sqrt{\dfrac{(3\rho_d + 2\rho_c)}{192\sigma}}$ $k_{br} = 0.2$ for bubble flow

Coalescence occurs due to the random collision of the bubbles/droplets. The source term s_{cl} for the bubble/droplet coalescence is expressed in general as follows,

$$s_{cl} = \int_0^\infty \int_0^\infty K_{cl}(d,d')\Delta S_\gamma^{cl}(d,d')n^2 P(d')dd'P(d)d(d) \tag{18}$$

where, $K_{cl}(d,d')$ is coalescence rate of bubble/droplet sizes d,d' and $\Delta S_\gamma^{cl}(d,d')$ is change in S_γ due to a single coalescence event of bubble/droplet sizes d,d'. Eq. (18) is simplified by

introducing assumptions that the volume of bubble/droplet is conserved during collision and the bubble size has a uniform distribution with an equivalent mean diameter d_{eq} as follows,

Table 3: Summary of Modelling for Coalescence Source Term

Viscous Collision	Inertial Collision
$k_{coll} = (8\pi/3)^{1/2}$ $u_{rel} = \dot{\gamma} d$ $P_{cl} = \exp(-t_d / t_i)$, $t_i = 1/\dot{\gamma}$ $t_d = \frac{\pi \mu_d \sqrt{F_i}}{2h_{cr}} \left(\frac{d_{eq}}{4\pi\sigma} \right)^{1.5}$ partial mobile interface for air/water flow $F_i = \frac{3\pi}{2} \mu_c \dot{\gamma} d_{eq}^w$, interaction force during collision $h_{cr} = \left(\frac{A_H d}{24\pi\sigma} \right)^{1/3}$, critical film thickness $A_H = 5 \times 10^{-21}$, Hamaker constant	$k_{coll} = (2\pi/15)^{1/2}$ $u_{rel} = (\varepsilon_c d_{eq})^{1/3}$ $P_{cl} = \frac{\Phi_{\max}}{\pi} \left(1 - \frac{k_{cl,2}^2 (We - We_o)^2}{\Phi_{\max}^2} \right)^{1/2}$ $\Phi_{\max} = \frac{2h_0^2 \rho_c \sigma}{We_o \mu_d^2 d}$ $k_{cl,2} \approx 11.0$ $We_o = 0.8 C_{WE} We_{cr}$ $h_0 = 8.3 h_{cr}$ $C_{WE} = 0.8$

$$s_{cl} = F_{cl}(2^{\gamma/3} - 2) \left(\frac{6\alpha_d}{\pi} \right)^2 k_{coll} u_{rel} P_{cl}(d_{eq}) d_{eq}^{\gamma-4} \tag{19}$$

where, $F_{cl}(=1.1)$ is the calibration coefficient, k_{coll} the collision rate coefficient, P_{cl} the coalescence probability of a single collision event. Each parameter is modelled according to the viscous and inertial collision regimes as summarized in the Table. 3. (See Lo et al., 2007, 2009)

The source term s_{mass} for mass transfer due to evaporation and condensation in the main flow is given by

$$s_{\gamma,mass} = \frac{dS_r}{dt} = \frac{\gamma}{3} \frac{S_\gamma}{\alpha \rho_g} \dot{m}_{mass} \tag{20}$$

where, $\dot{m}_{mass}$ is a mass transfer rate between the two phases.

The source term s_{boil} represents the generation of bubble at the wall due to boiling and is given by

$$s_{boil} = \frac{6 D_w^{\gamma-3}}{\pi \rho_g} \dot{m}_e \tag{21}$$

where, $\dot{m}_e$ is the mass generation rate by evaporation at the heated wall.

4. Benchmark Calculation and Result

4.1 Experimental Data

For the validation of the present advanced models, benchmark calculations were carried out against DEBORA experimental data (Garnier, 2001) by using STAR-CD 4.12. The test section is a vertical heated pipe of which the inner diameter is 19.2 mm. The total pipe length is 5*m* and it consists of three parts axially. The first part is an unheated section with a 1*m* length for the flow regulation at the inlet. The second part is a heated section with a 3.5*m* length for the simulation of wall boiling, and the third part located at the top region is an unheated section with a 0.5*m* length. The working fluid is R-12 and pressure of the experiment was in a range of 14.6~30 bars. The local two-phase flow parameters such as void fraction, bubble velocity, mean bubble diameter, liquid temperature and interfacial area concentration profiles were measured at the end of the heated section. One of the characteristics of DEBORA test is that the phasic density ratio is equivalent to that of steam/water around 90~170 bars and thus it is expected to represent the qualitative bubble behaviours in the high pressure steam/water condition. A total of 13 data sets were taken from three open literatures (Yao et al., 2004, Seiler al., 2008, Vyskocil et al., 2008) for the present benchmark calculation. The test cases are summarized in Table. 4.

Table 4: DEBORA Experimental Data and Their Experimental Conditions

Case Name	Pressure (bar)	G (kg/m^2/s)	T_{inlet}(^{o}C)	Q(W/m^2)	Reference
DEB5	26.15	1986	68.52	73890	Yao et al. (2004)
DEB6	26.15	1984.9	70.53	73890	
DEB10	14.59	2027.8	34.91	76240	
DEB13	26.17	2980.0	69.20	109420	
S1	14.59	2027	28.52	73161	Seiler et al. (2008)
S4	26.15	1985	70.53	72722	
Case1	30.06	1006.8	52.97	58260	Vyskocil et al. (2008)
Case2	30.06	1007.4	58.39	58260	
Case3	30.06	999.5	63.43	58260	
Case4	30.08	1005	67.89	58260	
Case5	30.07	1004.8	70.14	58260	
Case6	30.07	1004.8	72.65	58260	
Case7	30.06	994.9	73.7	58260	

4.2 Model Setup for the Simulation

Constitutive models such as interfacial drag, interfacial heat transfer, turbulence models, etc, should be provided for in the simulation of subcooled boiling flows by the Eulerian multiphase CFD codes. Most of these models have been already implemented into STAR-CD 4.12 and are selectable by the user. A detailed description of the basic models can be found in Lo (2005). In the present calculation, default turbulent dispersion force model (Gosman et al., 1992) with the value of *1* for the turbulent Prandtl number, Antal et al's (1991) wall lubrication force with the coefficients *-0.0167* and *0.147* for CW_o and CW_2, respectively, and constant lift force coefficients are applied. In addition to this, new models such as the Bozzano et al.'s (2001) interfacial drag model and Pfleger & Becker's (2001) two-phase turbulent model for k-ε equations are implemented into the user FORTRAN file to replace the existing models. In the calculation, k-ε equations is solved only for the continuous phase and turbulent diffusivity of disperse phase is correlated with that of the continuous phase.

4.3 Grid Sensitivity Study

In the present work, 2D equidistant grids were used in the simulation of the DEBORA test. DEB5 was selected among the 13 cases of DEBORA tests for the grid sensitivity study. Effects of radial grid size were studied by using 10, 15, 20, 25 and 30 grid cells in the radial direction while the axial grid cells are kept constant at 100. Fig. 3 shows simulation results according to the radial grid size. Here, bubble size is calculated from the fitting correlation based on the measured data. As shown in the figure, the result of local void fraction is insensitive to the radial grid size. However, the 10-node case shows that the bubble velocity is slightly lower than the others. From these results, 20 nodes are selected as the radial grid size. The sensitivity on the axial grid number is also studied using 100 and 200 grids along axial direction with 20 radial nodes. Fig. 3 also shows that the simulation results are insensitive to the number of axial nodes. From this investigation, 20 x 100 grids in the radial and axial directions are chosen as the basic grid size for all of the calculation.

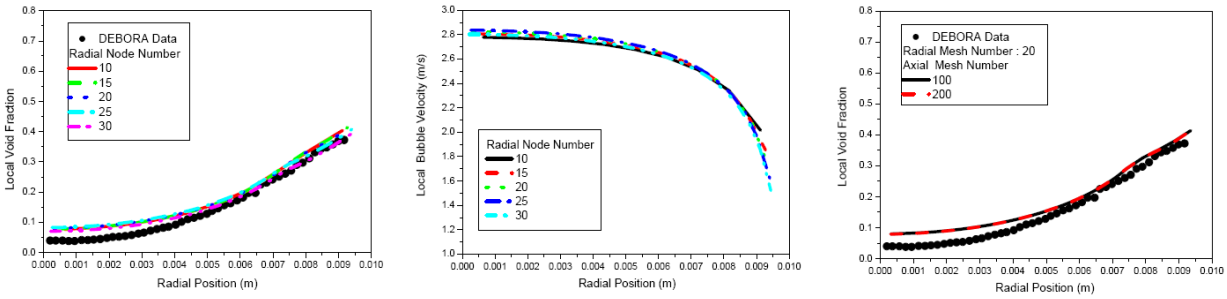

Fig. 3 : Grid Size Study with Default Wall Boiling Model (DEB5)

4.4 Results and Discussion

Calculations were performed according to 1) the default wall boiling model consisting of the Tolubinsky (1970) bubble departure size and Kurul & Podowski (1990) active nucleation site density models, 2) the advanced wall boiling model consisting of force balance bubble departure size and Hibiki et al.'s (2009) active nucleation site density models and 3) the advanced wall boiling model with the Sγ model. For the calculation of 1) and 2) above, a fitting equation for the bubble size obtained based on all of the DEBORA data is provided to eliminate its effect in the evaluation of wall boiling models. In the set up of coefficients for the wall boiling model, value for *FA* in eq. (2) is adjusted from 2 for default wall boiling model to 1 for the advanced wall boiling model. Here, velocity wall function for two-phase boiling flow described in section 2.2 was applied to all cases. A total of 13 test cases listed in the Table 4 were simulated by following the strategy given above, however, calculation results for just three cases are compared in Fig. 4.

The STAR-CD default wall boiling model predicted relatively higher local void fraction than the experimental data at all radial measurement locations of DEB5. Similar results are also shown in DEB6 case. The other 10 cases also showed that the default wall boiling model over-predicts slightly the local void fraction compared to the experimental data. In contrast, the advanced wall boiling model showed fairly good prediction results for all cases. In the calculation, the departure bubble size and active nucleation site density predicted by the advanced wall boiling model are at least ten times

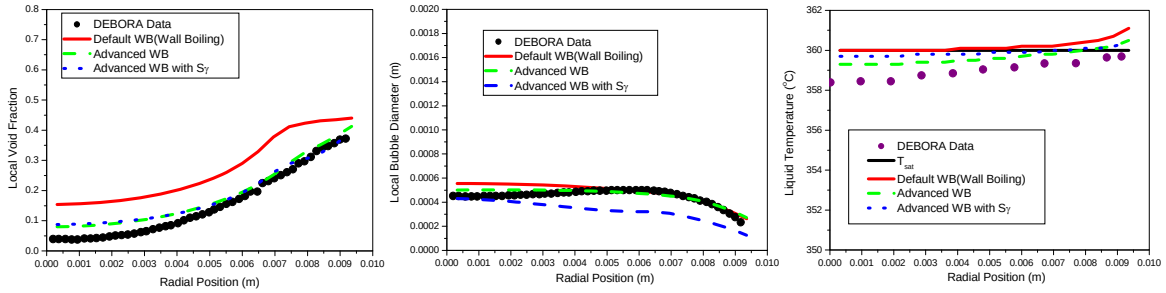

(a) DEB5

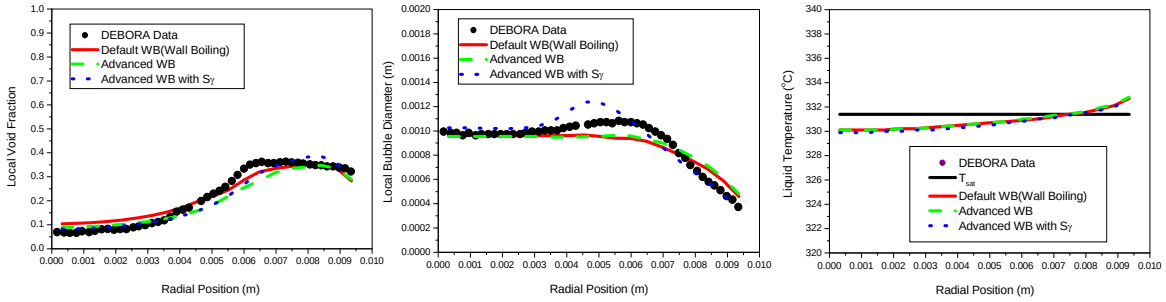

(b) DEB10

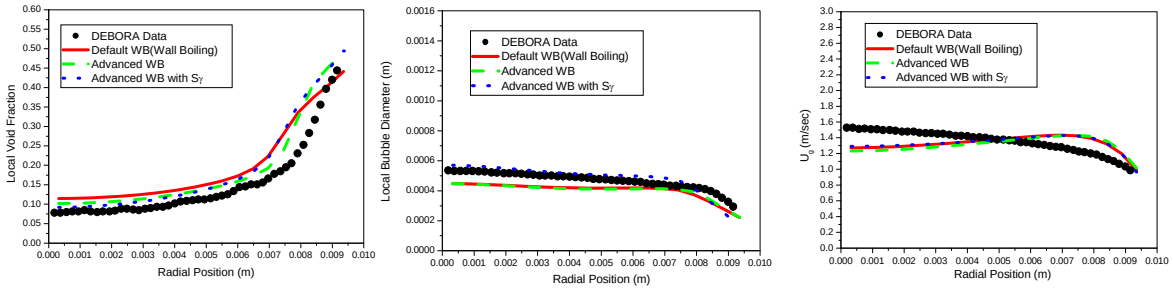

(c) Case 3

Fig.4 : Simulation Results for DEB5, DEB10 and Case3

smaller and several thousand times larger than those of the default wall boiling model. It is also worth noting that the two sub-models consisting of the advanced wall boiling model follows well the tendency on the flow condition, however the default wall boiling model results in the constant bubble departure size and active nucleation site density regardless of flow condition for all cases.

As shown in Fig. 4, the bubble size predicted by fitting equation follows well the experimental data as it is expected. For more mechanistic bubble size prediction, S_2 transport equation was solved with the advanced wall boiling model as expressed in equation (12) as well as S_1 equation for the log-normal distribution of bubble size. Figure 4 shows that the bubble size and its profile predicted by the S_γ model follows well the experimental data. Similar results were also found in the other ten cases.

The plots of liquid subcooling in Fig. 4 show that the default wall boiling model over-predicts liquid subcooling in the vicinity of the heated wall in case of DEB5, however the results from the advanced wall boiling model is improved.

In the data of "CaseN" series listed in Table 4, local bubble velocity is available from certain experimental data. Among them, the data for Case3 is compared with the prediction results as shown in the Fig. 4. The figure shows that a peak in the bubble velocity profile is found near the wall in contrary to the experimental data even though the velocity wall function for two-phase flow is applied. Similar trend is also observed in the calculation for Case2, 4 and 7. However, in other cases, the peak is not found near the heated wall and the predicted bubble velocity follows fairly well the trend of the experimental data. Remarkably, calculations without the two-phase wall function always show a peak near the heated wall for all test cases. It indicates that the two-phase wall function can improve the two-phase turbulent modelling, however it is not yet general enough to cover all flow conditions. There is much room for improvement in two-phase turbulence models.

5. CONCLUSIONS

In the present paper, a new advanced wall boiling model which consists of Klausner et al.'s force balance model for bubble departure size and Hibiki et al.'s active nucleation site model is proposed for the improvement of subcooled boiling model in CFD codes. The assessment against DEBORA experimental data showed that the advanced wall boiling model gives better prediction capability than the standard wall boiling model found in commercial CFD codes including STAR-CD. The advantages of the present wall boiling model are 1) it follows well the tendency in the change of flow conditions 2) it can be applicable to a wide range of flow conditions including nominal and postulated accidental conditions of nuclear power plant.

For the mechanistic prediction of bubble size, the Sγ model which was originally developed for the droplet flow was also applied in the subcooled boiling flow condition. The model coefficients for source and sink terms are readjusted based on the DEBORA experimental data. The benchmark calculation showed that the Sγ model can predict fairly well the DEBORA data.

It is also found that the velocity wall function for two-phase boiling flows can improve the prediction capability of phase velocity, however it is not the complete solution to improve two-phase turbulent modelling and there is much room for improvement in the modelling of two-phase turbulence.

REFERENCES

S.P. Antal, R.T.Lahey Jr., J.E. Flaherty, "Analysis of phase distribution in Fully Developed Laminar Bubbly Two-phase Flow", *Int. J. Multiphase Flow, Vol.* 17 (5), 450, pp. 635–652. (1991).

D. Bestion, H. Anglart, D. Caraghiaur, P. Péturaud, B. Smith, M. Andreani, B. Niceno, E. Krepper, D. Lucas, F. Moretti, M. C. Galassi, J. Macek, L. Vyskocil, B. Koncar, and G. Hazi, *Review of Available Data for Validation of Nuresim Two-Phase CFD Software Applied to CHF Investigations*, Science and Technology of Nuclear Installations, Volume 2009, Article ID 214512 (2009).

G. Bozzano, M. Dente, "Shape and Terminal Velocity of Single Bubble Motion: A Novel Approach", *Computer and Chemical Engineering*, Vol. 25, 571-576 (2001).

B.U. Bae, B.J. Yun, H.Y. Yoon, G.C. Park, C.-H. Song, "Analysis of Subcooled Boiling Flow with One-group Interfacial Area Transport Equation and Bubble Lift-off Model", *Nuclear Engineering and Design*, doi:10.1016/j.nucengdes.2010.04.001 (2010).

B.U. Bae, B.J. Yun, H.Y. Yoon, G.C. Park, C.-H. Song, "Development of Two-Phase Flow CFD Code With Interfacial Area Transport Equation For Analysis of Subcooled Boiling Flow", *XCFD4NRS*, Grenoble, France, 10 - 12 September (2008)

R. Cole, "A photographic study of pool boiling in the region of the critical heat flux", *AIChE J*. Vol.6, 533–542 (1960).

W.J. Duncan, A.S. Thom, A.D. Young, Mechanics of Fluids, Edward Arnold, 1972.

J. Garnier, E. Manon, G.Cubizolles, "Local measurements on flow boiling of refrigerant 12 in a vertical tube", Multiphase Sci. Technol. Vol. 13, pp. 1–111(2001).

A.D. Gosman, R.I. Issa, C., Lekakou, M.K. Looney, and S. Politis, "Multidimensional Modelling of Turbulent Two-phase Flows in Stirred Vessels", *AIChE Journal*, Vol.38 (12), pp.1946-1956 (1992)

T. Hibiki, M. Ishii, "Active Nucleation Site Density in Boiling Systems", *Int. J. Heat Mass Transfer* ,Vol. 46, pp. 2587-2601 (2009).

M. Ishii, Two-fluid model for two-phase flow, *Multiphase, Sci. Technol*. Vol. 5, 1–58 (1990)

M. Ishii, S. Kim, J. Kelly, "Development of interfacial area transport equation", *Nuclear Engineering and Technology*, Vol. **37**[6], pp. 525-536 (2005).

A.M. Kamp, A.K. Chesters, C. Colin, J. Fabre, "Bubble coalescence in turbulent flows: A mechanisitc model for turbulence-induced coalescence applied to microgravity bubbly pipe flow", International Journal of Multiphase Flow, Vol. **27**, pp.1363-1396 (2001).

I. Kataoka, A.Serizawa, "Analysis of turbulence structure of gas-liquid two phase flow under forced convective subcooled boiling", *Proceedings of the 2nd Japanese-German Symposium on Multi-phase Flow*, Tokyo, Japan (1997).

J. F. Klausner, R. Mei, D. M. Bernhard and L. Z. Zeng, "Vapor Bubble Departure In Forced Convection Boiling", *Int. J. Heat Mass Transfer*, Vol. 36, pp. 651-662 (1993).

B. Koncar, B. Mavko, "Modelling of Local Two-phase Flow Parameters in Upward Subcooled Flow Boiling with the CFX-4.3 Code", *IAEA-OECD/NEA Technical Meeting on Use of Computational Fluid Dynamics Codes for Safety Analysis of Reactor Systems*, Pisa, Italy, 11-14 Nov.(2002).

B. Koncar, B.Mavko, "Law of the Wall for Modelling of Subcooled Boiling Boundary Layer", *6th ICMF 2007*, Leipzig, Germany, 9-13 July (2007)

B. Koncar, E. Krepper, "CFD Simulation of Convective Flow Boiling of Refrigerant in a vertical Annulus", *Nuclear Engineering and Design*, Vol. 238, 693–706 (2008).

N. Kurul, M.Z.Podowski,"Multidimensional Effects in Forced Convection Subcooled Boiling", *Proceedings of the Ninth International Heat Transfer Conference*, Jerusalem, Israel, August, pp. 21–26 (1990).

S. Lo, Application of population balance to CFD modelling of bubbly flow via the MUSIG Model, AEA Technology, AEAT-1096 (1996).

S. Lo, "Modelling Multiphase Flow with an Eulerian Approach", *VKI Lecture Series – Industrial Two-Phase Flow CFD von Karman Institute*, May 23-27 (2005).

S. Lo, P. Rao, "Modelling of Droplet Breakup and Coalescence in an Oil-water Pipeline", *6th International Conference on Multiphase Flow, ICMF 2007*, Leipzig, Germany, July 9 – 13 (2007)

S. Lo and D. Zhang, "Modelling of Breakup and Coalescence in Bubbly Two-Phase Flows", *The Journal of Computational Multiphase Flows*, Vol.1 (1), pp.23-38 (2009).

D. Pfleger, S. Becker, "Modelling And Simulation Of The Dynamic Flow Behaviour In A Bubble Column", *Chemical Engineering Science*, Vol. 56 pp.1737-1747 (2001).

F.Ramstorfer, B. Breitschadel, H.Steiner, G.Breee,"Modelling of the Near-wall Liquid Velocity Field in Subcooled Boiling Flow", *Proc. ASME Summer Heat Transfer Conf.*, San Francisco, CA, July 2005, HT2005-71282 (2005)

H. Sakashita, "Measurement of nucleation site densities and bubble growth rates in saturated pool boiling of water at high pressures", *NURETH-13*, Kanazawa, Japan, September 27-October 2 (2009).

N. Seiler & P. Ruyer, "Advanced Model For Polydispersion in Size in Boiling Flows", *SHF :*

'écoulements diphasiques', Grenoble, France, 8-9 Septembre (2008).

R. Situ, T. Hibiki, M. Ishii, M. Mori, "Bubble Lift-off Size in Forced Convective Subcooled Boiling Flow ", *International Journal of Heat and Mass Transfer*,Vol. 48,pp. 5536–5548 (2005).

C-. H.Song, W. P. Baek, J. K. Park, "Thermal-hydraulic test and analyses for the APR1400's development and licensing", *Nuclear Engineering and Technology*, 39[4], 299-312 (2007).

V.I. Tolubinsky, D.M. Kostanchuk, "Vapour Bubbles Growth Rate and Heat Transfer Intensity at Subcooled Water Boiling Heat Transfer", 4th International Heat Transfer Conference, Paris, vol. 5, Paper No. B-2.8 (1970).

L. Vyskocil, J. Macek, "Boiling Flow Simulation in NEPTUNE CFD and Fluent Codes", *XCFD4NRS*, Grenoble, France, 10 - 12 September (2008)

W. Yao, C. Morel,"Volumetric interfacial area prediction in upward bubbly two-phase flow", *International Journal of Heat and Mass Transfer*, Vol 47, pp. 307–328 (2004)

G.H. Yeoh, J.Y. Tu, "A unified model considering force balances for departing vapour bubbles and population balance in subcooled boiling flow", *Nuclear Engineering and Design*, Vol. 235, 1251–1265 (2005).

B.J. Yun, D.J. Euh, C-.H. Song, " Investigation of the Downcomer Boiling Phenomena During The Reflood Phase of a Postulated Large-Break LOCA in the APR1400", *Nuclear Technology*, Vol. 156, 56-68 (2006).

B.J. Yun, A. Splawski, S. Lo, and C.–H. Song , "Advanced Wall Boiling Model with Wide Range Applicability for the Subcooled Boiling Flow and its Application into the CFD Code", Korea Nuclear Society Spring Meeting, Pyong-chang, Korea, 26-27 May (2010).

L. Z. Zeng, J. F. Klausner, and R. Mei, "A Unified Model for the Prediction of Bubble Detachment Diameters in Boiling Systems-I. Pool Boiling", *Int. J. Heat Mass Transfer*, Vol. 36. No. 9. pp. 2261-2270 (1993).

L. Z. Zeng, J. F. Klausner, D. M. Bernhard and R. Mei, "A Unified Model for the Prediction of Bubble Detachment Diameters in Boiling Systems-II. Flow Boiling", *Int. J. Heat Mass Transfer*, Vol. 36. No. 9. pp. 2271-2279 (1993).

N. Zuber, "The Dynamics of Vapor Bubbles in Nonuniform Temperature Fields", *Int. J. Heal Mass Transfer*. Vol. 2, pp. 83-98 (1961).

ACKNOWLEDGMENTS

The work presented was carried out at the Didcot office of CD-adapco in the UK during the sabbatical year of B.J. Yun. This work was supported by the Nuclear Research & Development Program of the NRF (National Research Foundation of Korea) grant funded by the MEST (Ministry of Education, Science and Technology) of the Korean government (Grant code: M20702040003-08M0204-00310).